

# The $\delta$ Scuti star FG Virginis

## IV. Mode identifications and pulsation modelling

M. Breger<sup>1</sup>, A.A. Pamyatnykh<sup>1,2,3</sup>, H. Pikall<sup>1</sup>, and R. Garrido<sup>4</sup>

<sup>1</sup> Astronomisches Institut der Universität Wien, Türkenschanzstrasse 17, A-1180 Wien, Austria (e-mail: breger@astro.univie.ac.at)

<sup>2</sup> Copernicus Astronomical Center, Bartycka 18, PL-00-716 Warsaw, Poland

<sup>3</sup> Institute of Astronomy, Russian Academy of Sciences, Pyatnitskaya Str. 48, 109017 Moscow, Russia

<sup>4</sup> Instituto de Astrofísica de Andalucía, CSIC, Apdo. 3004, E-18080 Granada, Spain

Received 5 August 1998 / Accepted 20 October 1998

**Abstract.** This paper examines the mode identification and presents pulsation models for FG Vir, for which 24 frequencies have been detected. Histograms of the frequency spacings show peaks which are identified with adjacent radial orders and rotational splitting.

Pulsational  $\ell$  values are deduced for eight modes by comparing the observed photometric phase lags between  $v$  and  $y$  variations with calculated values. The dominant pulsation mode at 12.72 c/d can be identified with  $\ell = 1$ , while the 12.15 c/d mode is the radial fundamental. These results are in agreement with identifications published by Viskum et al. (1998).

Based on the observational mode identifications and the Hipparcos distance, new models were computed with the constraint that the mode at 12.15 c/d is the radial fundamental mode. It is shown that with standard opacities, models in the appropriate  $T_{\text{eff}}$ ,  $\log L$  and  $\log g$  ranges cannot reproduce the identification in the literature of 23.40 c/d as the third radial overtone. However, we show that observationally an  $\ell = 1$  (rather than radial) identification is equally probable.

A large number of pulsation models were computed for FG Vir. A comparison between the observed frequencies and mode identifications and pulsation models leads to a mean density of  $\bar{\rho}/\bar{\rho}_{\odot} = 0.156 \pm 0.002$  depending on the opacity and chemical composition choice and on the possible overshooting from the convective core. The models also correctly predict the observed region of instability between 9 and 34 c/d.

The effect of rotational coupling on the pulsation frequencies is estimated.

**Key words:** stars: individual: FG Vir – stars: oscillations – stars: variables:  $\delta$  Sct

### 1. Introduction

FG Vir (=HD 106384) is a  $\delta$  Scuti variable near the end of its main-sequence evolution. 435 hours of photometric measurements by the Delta Scuti Network determined 24 statistically

significant frequencies from 9.20 to 34.12 c/d (106 to 395  $\mu$ Hz). Details of this campaign as well as references to earlier measurements and results can be found in Breger et al. (1998). The large number of detected pulsation modes makes this star an excellent candidate for asteroseismological investigations. This requires the identifications of the observed pulsation frequencies with specific pulsation modes. While the problem is rather complex, considerable progress has been achieved, as shown by Breger et al. (1995), Guzik et al. (1998) and Viskum et al. (1998).

The pulsation mode identification from observed frequencies requires accurate determinations of the basic parameters of the star. From the available  $wby\beta$  photometry, Mantegazza et al. (1994) derived  $T_{\text{eff}} = 7500$  K and  $\log g = 3.95$ . A correction for a misprint in the literature leads to a correction of  $\log g$  to 3.9. We can now improve these values further by including the accurate Hipparcos parallax which predicts  $M_V = 1.95 \pm 0.13$  mag. This is slightly fainter than the value of  $1.71 \pm 0.25$  mag predicted by  $wby\beta$  photometry. This leads to a corresponding shift in  $\log g$  to 4.00. These values are in exact agreement with those derived by Viskum et al. (1998). We estimate the uncertainties to be  $\pm 100$  K in temperature and  $\pm 0.1$  in  $\log g$ .

The values of the pulsation constants  $Q$  can be estimated from the following empiric equation:

$$\log Q_i = -6.456 + \log P_i + 0.5 \log g + 0.1 M_{\text{bol}} + \log T_{\text{eff}}.$$

The constant,  $-6.456$ , in the above formula is based on solar values of  $M_{\text{bol}} = 4.75$  mag,  $B.C. = -0.08$  mag,  $T_{\text{eff}} = 5770$  K and  $\log g = 4.44$ . If the  $Q$  values are calculated from  $wby\beta$  photometry, the observational uncertainties in observing these parameters lead to an uncertainty in  $Q$  of about 18%.

The corresponding  $Q$  values are shown in Table 1.

### 2. Regularities of frequency spacing

The values of the observed frequencies and regularities in their patterns can be an excellent initial tool for mode identifications, if enough frequencies are excited and detected. For high-order, low-degree p-mode pulsation, the different radial orders show

Send offprint requests to: M. Breger

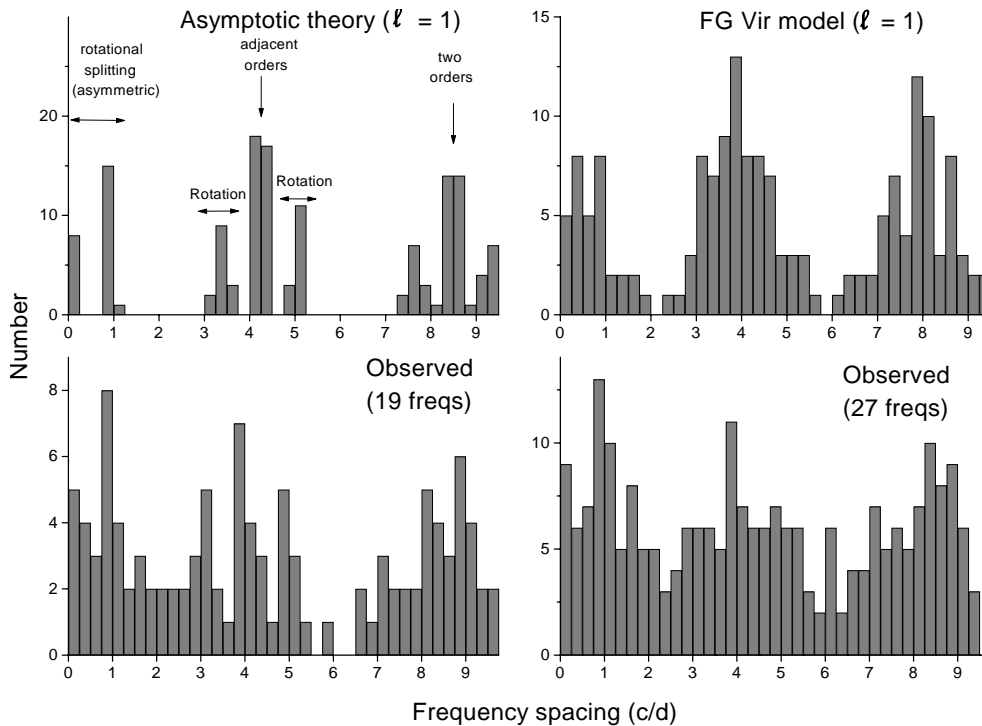


**Fig. 1.** Histograms of frequency spacing between all specified pulsation modes. *Top left:* The diagram demonstrates that for high orders the patterns of frequency spacing clearly show adjacent radial orders ( $\sim 4$  c/d) and the effects of rotational splitting, which is extremely asymmetric even at  $V_{\text{rot}} = 45$  km/s. *Top right:* The frequency spacing predicted from model 1 for  $\ell = 1$  in the observed frequency range of 11 – 35 c/d. Note that the patterns from adjacent orders and rotational splitting are still present. *Bottom panels:* Observed frequency spacings in the observed range from 11 to 35 c/d. Although these are a mixture of  $\ell = 0, 1$  and  $2$  modes, the effects of adjacent radial orders and a small peak in the range of rotational splitting can be seen. To demonstrate that the results are not sensitive to which observed frequencies are included, two different choices (see text) are shown

uniform frequency spacing, with a mode of order  $n$  and of degree  $\ell$  being shifted from the corresponding mode  $(n, \ell + 1)$  by half of the frequency difference between the  $(n, \ell)$  and  $(n + 1, \ell)$  modes (Vandakurov 1967). In  $\delta$  Scuti stars, the excited pulsation modes are of low order ( $n$  up to 7), so that the asymptotic relations do not apply exactly. Nevertheless, they also show some regularities. Additionally g-modes invade the p-mode region and decrease the spacing in a small frequency region of about two radial orders. This effect, known as avoided crossing (Osaki 1975, Aizenman, Smeyers & Weigert 1977), complicates the theoretical frequency spectra, but can provide information about the stellar interior (Dziembowski & Pamyatnykh 1991). Moreover, stellar rotation splits multiplets and this splitting is non-symmetric, if second-order effects of rotation and effects of rotational mode coupling are taken into account (Dziembowski & Goode 1992, Soufi et al. 1998, Pamyatnykh et al. 1998). Nevertheless, the spacing of adjacent radial orders as well as the rotational splitting is still regular enough to be detectable, if complete multiplets are excited and identified. We will demonstrate this by using a pulsation model of a  $1.85 M_{\odot}$  star with  $T_{\text{eff}} = 7515$  K,  $\log g = 3.99$ , and  $V_{\text{rot}} = 45$  km/s. This model will be referred to as model 1. The parameters for the model were not chosen at random, but can be regarded as an estimate for FG Vir.

To investigate the period regularities, Winget et al. (1991) have successfully applied the method of the Fourier transform of the period spacing to the star PG 1159+035. This method requires coherence over a large frequency range. Handler et al. (1997) also found frequency regularities from Fourier transformations of the frequency spectrum of the unevolved  $\delta$  Scuti star

XX Pyx. Since strict equidistant frequency or period spacing is not expected for FG Vir, the method is not optimal for this  $\delta$  Scuti star. Instead, we use a method which does not require such a coherence: an examination of a histogram of the observed frequency differences between all detected frequencies. In such a diagram, regularities in the frequency spacing of adjacent radial orders of modes with the same degree,  $\ell$ , should show up as a peak. Furthermore, modes of different degree are shifted in frequency relatively to each other, but would still have similar patterns and, therefore, contribute to the peaks in the histogram.

The frequency spacing is examined in Fig. 1 with both the theoretically predicted and observed spacings. Pulsation models show a typical frequency spacing of  $\Delta f \approx 4$  c/d for adjacent radial orders of p-modes, independent of the degree of the modes. The leftmost peaks in the top panels of Fig. 1 are caused by rotationally split multiplets. A similar diagram for  $\ell = 2$  (not plotted separately) does not show such strong peaks in the expected region. The reason is that both the presence of g-modes in addition to the p-modes and non-equidistant rotational splitting significantly disturb the regularity in the distribution of quadrupole mode frequencies (see Fig. 7 below.) As a result, the combined pattern of frequency spacings for all  $\ell = 0 - 2$  modes becomes much less clear. Moreover, due to the fact that only low-order oscillations are present in this frequency range, there is no additional peak at  $\Delta f \approx 2$  c/d as might be expected from the asymptotic spacing between p-modes of adjacent degrees (see Fig. 7 for more details).

Next, we turn to the observed frequency spacing for the 24 certain and 8 probable frequency detections of FG Vir (Table 1). The most cautious approach would be to use the 24 certain fre-

**Table 1.** Pulsation frequencies of FG Vir

	Frequency c/d	$\mu\text{Hz}$	1995 V amplitude mmag	Q value days
Statistically significant frequencies				
$f_1$	12.716	147.2	21.1	.0323
$f_2$	24.228	280.4	4.5	.0170
$f_3$	23.403	270.9	4.1	.0176
$f_4$	21.052	243.7	3.7	.0195
$f_5$	19.868	230.0	3.5	.0207
$f_6$	12.154	140.7	3.5	.0338
$f_7$	9.656	111.8	3.4	.0426
$f_8$	9.199	106.5	3.1	.0447
$f_9$	19.228	222.5	1.5	.0214
$f_{10}$	20.288	234.8	1.3	.0203
$f_{11}$	24.200	280.1	1.3	.0170
$f_{12}$	16.074	186.0	1.0	.0256
$f_{13}$	34.119	394.9	1.0	.0121
$f_{14}$	21.232	245.7	1.0	.0194
$f_{15}$	11.110	128.6	0.9	.0370
$f_{16} = 2f_1$	25.432	294.4	0.9	.0162
$f_{17}$	33.056	382.6	0.6	.0124
$f_{18}$	21.551	249.4	0.8	.0191
$f_{19}$	28.140	325.7	0.6	.0146
$f_{20}$	11.195	129.6	0.7	.0367
$f_{21}$	24.354	281.9	0.6	.0169
$f_{22}$	11.870	137.4	0.4	.0346
$f_{23} = f_1 + f_7$	22.372	258.9	0.5	.0184
$f_{24} = f_3 - f_1$	10.687	123.7	0.5	.0385
Probable frequencies				
$f_{25}$	25.37	293.7	0.4	.0162
$f_{26}$	25.18	291.4	0.4	.0163
$f_{27}$	29.50	341.4	0.4	.0139
$f_{28}$	18.16	210.2	0.4	.0226
$f_{29}$	19.65	227.4	0.4	.0209
$f_{30}$	31.92	369.4	0.4	.0129
$f_{31}$	20.83	241.1	0.4	.0197
$f_{32}$	12.79	148.1	0.4	.0322

quencies with a few exceptions: the  $2f_1$  term at 25.4 c/d (reflecting the departure from a pure sinusoidal light curve shape of  $f_1$ ), the two combination frequencies (the pulsation models cannot yet predict which combinations and resonances are excited), and the two low-frequency modes for which the p-mode character can definitely be excluded from the assumption that  $f_6$  is the radial fundamental mode. To show that the agreement between the theoretically predicted and observed frequency spacing is not based on the choice of frequencies, the analysis was repeated by including the 8 additional ‘probable’ modes listed in Table 1.

To conclude, the theoretical and observed frequency spacings agree quite well. In particular, for frequency differences in the 0 – 5 c/d range, two features near 3.9 and 0.8 c/d stand out, suggesting an identification with the spacing of successive radial orders and rotational splitting, respectively.

### 3. Pulsation mode identifications from photometric phase differences

The relative phase difference between the temperature and radius variations of a pulsating star leads to an observable phase difference between the light curves at different wavelengths. The sizes of these phase differences depend not only on the properties of the star, but also on the type of pulsation mode. The observed phase difference can then be used for mode typing. This was already pointed out by Watson (1988). Garrido et al. (1990) presented detailed calculations and predictions for  $\delta$  Scuti stars. They find that measurements through different filters of the Strömgren *uvby* system provide discrimination between radial and low-order nonradial pulsation, i.e. help determine the  $\ell$  value<sup>1</sup>.

We have chosen the *v* and *y* filters to provide a relatively large baseline in wavelength. The *u* filter was not used by us because of the very large potential for systematic observational errors. These details of the measurements can be found in Breger et al. (1998). The phase differences were determined in the following manner: The values of the 24 known and well-determined frequencies were optimized by making a common solution of the available *y* data from 1992 – 1996, while allowing for the amplitude variability of  $f_3$ . As discussed in Breger et al., all CCD measurements were given a weight of 0.19. With these optimized frequencies, for the year 1995 the best amplitudes and phases were calculated from the available 412 hours of *y* and 292 hours of *v* data. Separate trial solutions indicate that the resulting phase differences are relatively insensitive to the weights adopted. For the year 1996, an additional 82 hours of *uvby* photometry are available (Viskum et al. 1998). The data were combined with the larger data set from 1995 while allowing for variable amplitudes of  $f_3$ . We note that the calculated uncertainties of the phase differences are not reduced by including the additional data: the reason is that the 1995 data have smaller deviations, e.g. 4 vs. 6 mmag in *v*.

The resulting phase differences are shown in Table 2. The phase errors (in degrees) were estimated from the formula  $\sigma(\phi) = 180/\pi \cdot \sigma(m)/a$ , where  $a$  is the amplitude and  $\sigma(m)$  is the uncertainty of each data point (average deviation per point from the fit).

We can now compare the observed phase differences with theoretical modelling in order to determine the  $\ell$  values. The ATLAS9 models of Kurucz (1993) were used to construct a model atmosphere for FG Vir. Garrido et al. (1990) presented calculations using values of  $\Phi^T$  ranging from 90° to 135°. For FG Vir, Viskum (1997) determined a smaller range, viz.  $\Phi^T = 126^\circ \pm 20^\circ$ . This allowed us to refine the calculations, although the results are very similar. Another required constant, the deviation from adiabaticity,  $R$ , has been changed slightly

<sup>1</sup> It is necessary to note that rotational mode coupling may enlarge the overlapping between modes of different  $\ell$  values in the amplitude-phase diagrams, as it was discussed by Pamyatnykh et al. (1998): for example, a quadrupole mode coupled by rotation with the closest radial mode may be shifted in such a diagram towards the region occupied by dipole modes.

**Table 2.** Phase differences and mode identifications of FG Vir

	Frequency		Phase differences in degrees		Pulsation degree, $\ell$	
	c/d	$\mu\text{Hz}$	$\phi_v - \phi_y$		Spectroscopy	Photometry
			1995	1995/6	Viskum et al. (1998)	Present
$f_1$	12.716	147.2	$-1.0 \pm 0.2$	$-1.3 \pm 0.2$	1	1
$f_2$	24.228	280.4	$-3.0 \pm 1.1$	$-3.8 \pm 1.1$	1	1, 2
$f_3$	23.403	270.9	$-0.6 \pm 1.2$	$-1.1 \pm 1.2$	0	0, 1
$f_4$	21.052	243.7	$-5.7 \pm 1.4$	$-7.1 \pm 1.5$	2	2
$f_5$	19.868	230.0	$-4.9 \pm 1.4$	$-5.5 \pm 1.5$	2	2
$f_6$	12.154	140.7	$+6.8 \pm 1.4$	$+5.5 \pm 1.4$	0	0
$f_7$	9.656	111.8	$-2.2 \pm 1.4$	$-2.7 \pm 1.4$	2	1, 2
$f_8$	9.199	106.5	$-4.4 \pm 1.6$	$-7.6 \pm 1.7$	2	2
Number of hours $y/v$			412/292	494/374		

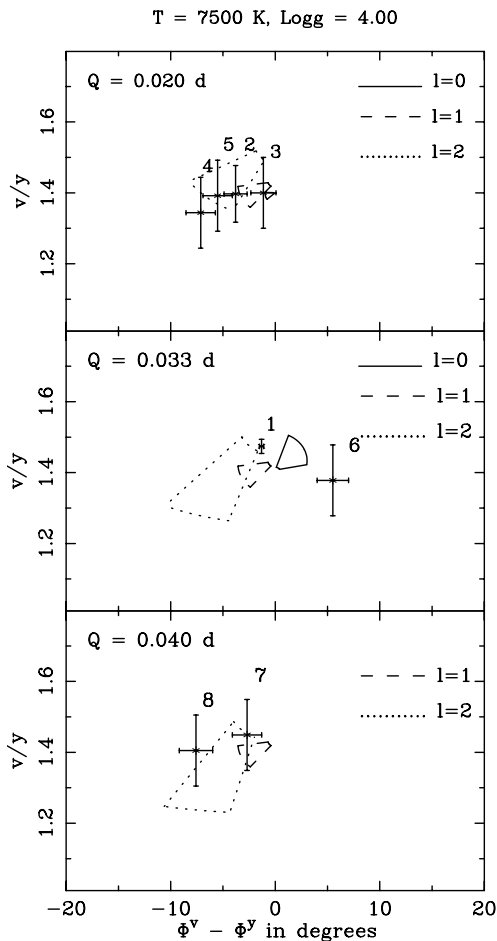


**Fig. 2.** Diagnostic diagram to determine  $\ell$  values of FG Vir from Strömgren  $v$  and  $y$  colors. The axes represent amplitude ratios and phase differences. Measurements are shown by crosses with error bars, while the four-sided loops represent the models (see text). The three panels represent the pulsation modes with different values of the pulsation constant,  $Q$

from the value used by Garrido et al. (1990). Values of 0.20 (instead of 0.25) to 1.00 were used. This change was indicated by measurements of high-amplitude  $\delta$  Scuti stars. The theoretical

predictions are shown in Fig. 2 together with the observations. The importance of considering the dependence on the pulsation constant,  $Q$ , can be seen for  $Q = 0.02$ , where one can even find negative values of the phase difference for radial modes, although the separation between radial and nonradial modes is always maintained.

Our best mode identifications based on Strömgren photometry are shown in Table 2. We obtained five unambiguous  $\ell$  values, while for three further modes we cannot distinguish between two adjacent  $\ell$  values. The frequency  $f_6$ , shown in the middle panel, is situated to the right of the  $\ell = 0$  by  $1.9 \sigma$ . We note that the deviation is caused by only one subset of data (the CCD measurements from Siding Spring Observatory, see Stankov et al. 1998), without which a phase shift of  $+3.7^\circ$  is found. Irrespective of which of the two values for  $f_6$  is accepted, an identification with radial pulsation is consistent within the statistical uncertainties.

We can now compare the results from the photometric method with those derived from a promising new technique of examining the equivalent width variations of selected lines. Bedding et al. (1996) have shown that for low degree pulsation, the  $\ell$ -values of pulsation modes can be inferred from simultaneous observations of several selected absorption lines combined with simultaneous photometric observations. Viskum et al. (1998) have applied this method to the star FG Vir. In particular, the equivalent-width changes of the  $H\alpha$  and  $H\beta$  lines turned out to be good discriminators. In their paper,  $\ell$  identifications have been presented for the eight dominant modes.

We note that on the observational side the photometric and spectroscopic methods are independent. However, both methods rely on similar model-atmosphere calculations, so that they cannot be considered to be completely independent of each other.

The agreement between the photometric and spectroscopic mode determinations is remarkable. It appears prudent to examine the comparison of the results of the two methods in more detail, especially with consideration of the (unavoidable) observational uncertainties. In order to compare independent parameters with each other, we pick the amplitude ratio of  $A(H\alpha)/A(FeI)$  given by Viskum et al. (1998). The comparison is shown in Fig. 3, where the numbers next to the points refer

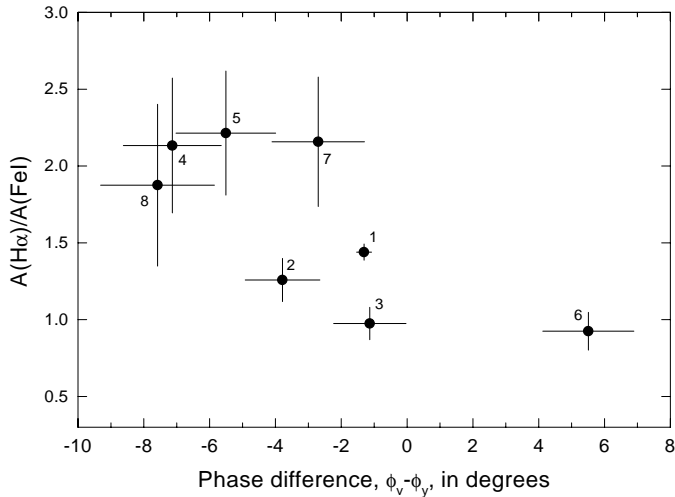


**Fig. 3.** Comparison of the equivalent-width and photometric methods to determine  $\ell$  values. Radial pulsation ( $\ell=0$ ) can be found in the lower right,  $\ell=1$  in the middle, while  $\ell=2$  is found near the top left. The diagram shows that the two methods are in agreement, but also demonstrates that some of the agreement may be accidental once the error bars are taken into consideration

to the frequency numbering in Table 1. The figure shows that some of excellent agreement may be accidental once the observational uncertainties are considered. Nevertheless, the viability of both methods to determine  $\ell$  values has been demonstrated and for at least six modes the  $\ell$  values have been observationally determined. These determinations now need to be used as input for pulsation models.

#### 4. Pulsation models for FG Vir

Since the initial discovery of multiperiodicity of FG Vir, several studies attempted to fit the observed and theoretical frequency spectra of the star, viz. Breger et al. (1995), Guzik, Templeton & Bradley (1998), and Viskum et al. (1998). We will now calculate new models utilizing the newly discovered pulsation frequencies and mode identifications.

##### 4.1. Method of computation

To compute models of FG Vir we used a standard stellar evolution code which was developed in its main parts by B. Paczyński, M. Kozłowski and R. Sienkiewicz (private communication). The same code was used in our recent studies of period changes in  $\delta$  Scuti stars (Breger & Pamyatnykh 1998) and in a seismological study of XX Pyx (Pamyatnykh et al. 1998). These two papers include detailed descriptions of the model computations, so that the present description can be brief. For the opacities, we used the latest version of the OPAL or the OP tables (Iglesias & Rogers 1996 and Seaton 1996, respectively) supplemented with the low-temperature data of Alexander & Ferguson (1994). In all computations the OPAL equation of state was used (Rogers et al. 1996).

The computations were performed starting with chemically uniform models on the ZAMS, assuming typical Population I values of hydrogen abundance,  $X$ , and heavy element abundance,  $Z$ . The initial heavy element mixture of Grevesse & Noels (1993) was adopted.

In some models, a possibility of overshooting from the convective core was taken into account. The overshooting distance,  $d_{\text{over}}$ , was chosen to be  $0.2 H_p$ , where  $H_p$  is the local pressure scale height at the edge of the convective core. Examples of evolutionary tracks for  $\delta$  Scuti models computed with and without overshooting are given in Breger & Pamyatnykh (1998).

In the stellar envelope the standard mixing-length theory of convection with the mixing-length parameter  $\alpha = 1.0$  or  $2.0$  was used. As we will see below, the choice of the mixing-length parameter  $\alpha$  has only a small effect on our models, because they are too hot to have an effective energy transfer by convection in the stellar envelope.

In all computations we assumed uniform (solid-body) stellar rotation and conservation of global angular momentum during evolution from the ZAMS. These assumptions were chosen due to their simplicity. The influence of rotation on the evolutionary tracks of  $\delta$  Scuti models was demonstrated by Breger & Pamyatnykh (1998). We studied models of FG Vir with equatorial rotational velocities from, approximately, 30 to 90 km/s (on the ZAMS, the values are 5-10 km/s higher). This range is consistent with the values of  $v \sin i = 21 \pm 1$  km/s and  $i = 31^\circ \pm 5^\circ$  found by Mantegazza et al. (1994) and an equatorial velocity of  $33 \pm 2$  km/s obtained by Viskum et al. (1998). At such low rotational velocities, the evolutionary tracks are located very close to those for non-rotating stellar models. The main effect of rotation to be considered is the splitting of multiplets in the oscillation frequency spectra. This splitting is non-symmetric even for slowly rotating stars, if second-order effects are included.

The linear nonadiabatic analysis of low-degree oscillations ( $\ell \leq 4$ ) was performed using the code developed by Dziembowski (1977). In the modern version of the code, effects of slow stellar rotation on oscillation frequencies are taken into account up to second order in the rotational velocity (Dziembowski & Goode 1992, Soufi et al. 1998).

##### 4.2. Model constraints using oscillation data

The models for FG Vir were constructed with the observed mode  $f_6$  (12.154 c/d) being identified with the radial fundamental mode ( $=\mathbf{F}$ ) (see Sect. 3). Note that this determines the mean density of all possible models of FG Vir: with the pulsation constant of about 0.032–0.034 days, which is typical for  $\delta$  Scuti variables, we obtain  $\bar{\rho}/\bar{\rho}_\odot \approx 0.15$ –0.17. A considerably more accurate value of the density will be obtained later in this section.

We started with the construction of evolutionary tracks of  $1.75$ – $1.95 M_\odot$  models for initial abundances  $X = 0.70$  and  $Z = 0.02$  and using OPAL opacities. No overshooting from the convective core was allowed. The initial equatorial rotational velocity on the ZAMS was chosen to be 50 km/s. With our assumption of conservation of global angular momentum, the equato-

rial rotational velocity is decreasing during the MS–evolution from 50 km/s at the ZAMS to about 40–41 km/s at the TAMS (Terminal–Age–Main–Sequence). The evolutionary tracks are shown in Fig. 4 together with the range in effective temperature and gravity of FG Vir (see Introduction) derived from photometric calibrations ( $T_{\text{eff}} = 7500 \pm 100$  K and  $\log g = 4.00 \pm 0.10$ ). This range requires MS models and constrains the mass of the models to 1.75–1.95  $M_{\odot}$ . The position of the models, whose **F**-mode has a value of 12.154 c/d is also shown. This further constrains the mass to 1.815–1.875  $M_{\odot}$ . We stress that this strong seismological mass constraint depends on an accurate effective temperature determination.

The identification of  $f_6 \equiv \mathbf{F}$  agrees well with the gravity estimate for FG Vir. This provides no additional constraints on the stellar mass since the lines of constant frequencies are approximately parallel to those of constant gravity, as shown in the lower panel of Fig. 4.

For a given family of stellar models, the radial fundamental pulsation constant,  $Q$ , is constant with a quite high accuracy due to the homologous structure of models of different masses. For  $M = 1.80 - 1.90 M_{\odot}$  in the range  $\log T_{\text{eff}} = 3.869 - 3.881$  ( $T_{\text{eff}} = 7400 - 7600$  K), the pulsation constant  $Q = 0.0326$  with relative accuracy of about 0.2%. The accuracy will be still higher by approximately one order of magnitude if we consider only models based on  $f_6 \equiv \mathbf{F}$ . For these models we determine a mean density of  $\bar{\rho}/\bar{\rho}_{\odot} = 0.1570 \pm 0.0001$ . However, such an extremely high accuracy is based on a fixed choice of input physics: stellar opacity, initial chemical composition, rotational velocity and parameters of convection. We will see in the next subsection that changing these parameters results in significantly larger spread of mean density for FG Vir models.

The strict constraint on mass is demonstrated in Fig. 5, where the changes of radial and dipole frequencies during MS evolution are shown. This agreement is an independent qualitative argument in favour of the proposed models for FG Vir. Another important result is the good agreement of the predicted frequency range of unstable modes with the observed frequency range of 9–34 c/d. An additional test shows that should we identify  $f_6$  with the first radial overtone instead of the **F**-mode, we cannot achieve agreement between the theoretical and observed frequency ranges: in the corresponding models of  $\approx 2.0 M_{\odot}$  the instability occurs in the frequency range of 8–30 c/d. The tendency in models of higher mass to shift the instability range to lower frequencies can be also seen in Fig. 5. There is an even stronger argument against these higher-mass models: their luminosities are too high ( $\log(L/L_{\odot}) \sim 1.3$ ) to be consistent with both the photometric calibrations and the Hipparcos parallax.

A number of gravity modes must be excited in FG Vir, if the assumption of  $f_6 \equiv \mathbf{F}$  is true, because the two lowest frequencies are more than 25% lower than the **F**-mode. Moreover, during the MS-evolution the frequencies of low-order g-modes increase and approach consecutively the frequencies of low-order p-modes resulting in mode interactions and avoided crossings (see Unno et al. 1989 and references therein). The frequency spectrum is much more complicated than in the case of pure p- or g-modes, as shown in Fig. 5 for dipole modes.

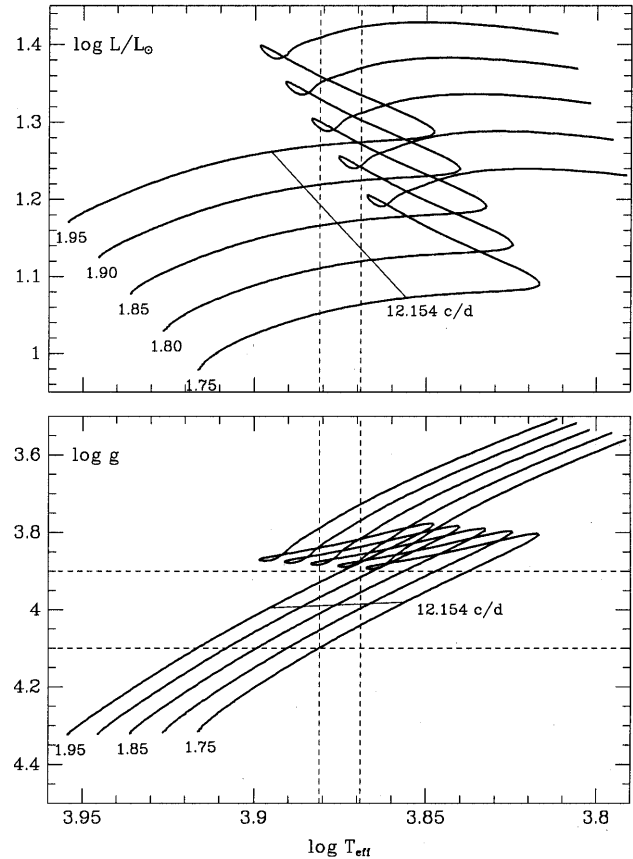


**Fig. 4.** Evolutionary tracks of 1.75–1.95  $M_{\odot}$  standard models. The equatorial rotational velocity on the ZAMS was chosen to be 50 km/s. On the TAMS (at the turn-off points to the left), equatorial velocities are of about 40–41 km/s. Dashed lines show effective temperature and  $\log g$  ranges of FG Vir from photometric calibrations. The thin solid line connects models whose radial fundamental mode frequency is 12.154 c/d. The rotational velocity of the models along this line is about 45 km/s

The avoided crossing phenomenon takes place approximately in the middle of the observed frequency interval. Therefore, most of the excited modes at these and at lower frequencies are of mixed character: they behave like p-modes in the envelope and like g-modes in the interior. In the 1.85  $M_{\odot}$  model with  $\log T_{\text{eff}} = 3.876$ , modes  $g_1$ ,  $p_2$  and  $p_3$  are of mixed character. The frequencies of modes at avoided crossing are sensitive to the structure of the deep stellar interior. Consequently, the detection of these modes is important for testing convective overshooting theories (Dziewbowski & Pamyatnykh 1991).

Avoided crossings for quadrupole modes in the models of FG Vir occur close to the upper border of the observed frequency interval and also close to the **F**-mode. This means that most of  $\ell = 2$  p-modes in the interval already interacted with gravity modes and are of mixed character.

#### 4.3. Effects of different input parameters on the FG Vir models

The 1.85  $M_{\odot}$  model for FG Vir, which was discussed in the previous subsection, will be referred to as the standard or ref-

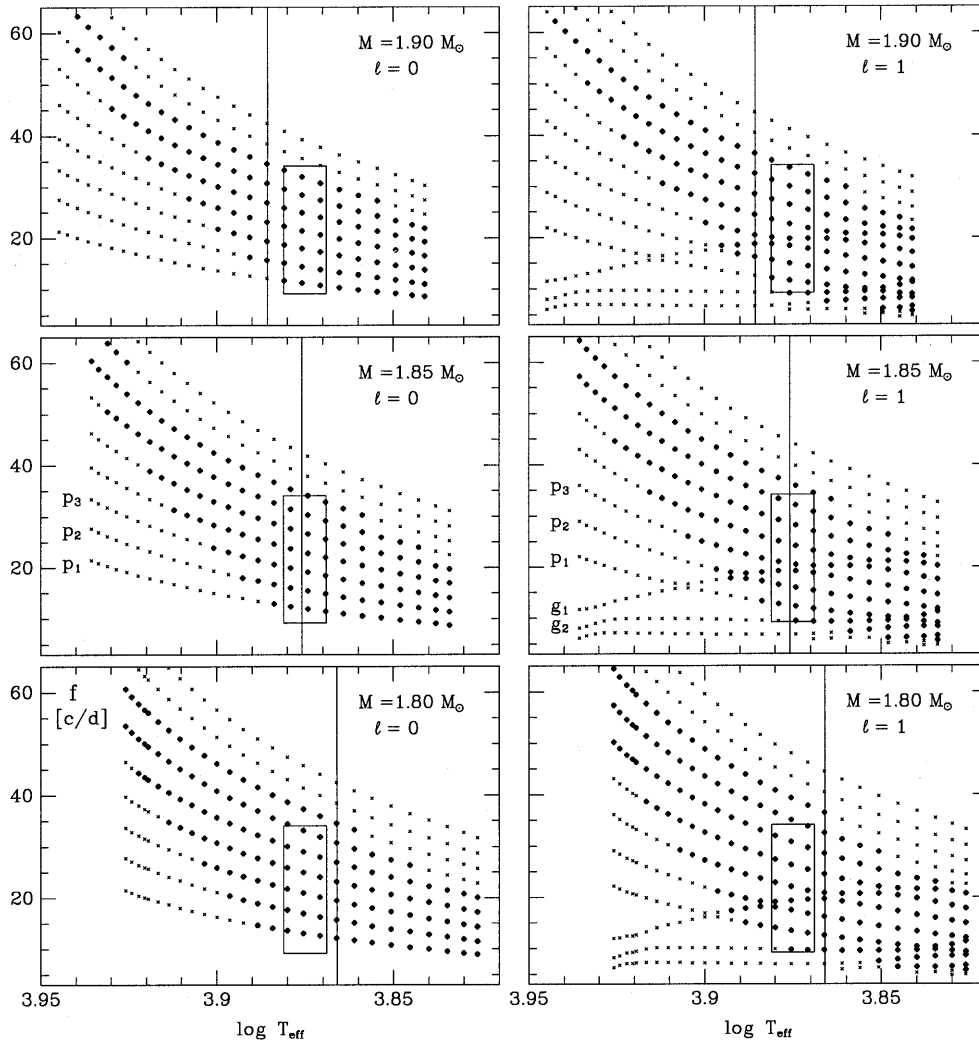


**Fig. 5.** Main-sequence evolution of low-order frequency spectra of radial and dipole oscillations of stellar models with masses 1.80, 1.85 and  $1.90 M_{\odot}$ . In each panel, leftmost and rightmost points correspond to the ZAMS and to the TAMS models, respectively. Large filled circles denote unstable modes. For simplicity, for  $\ell = 1$  only axisymmetric ( $m = 0$ ) components of the dipole multiplets are shown. Rectangular boxes mark the observational frequency and effective temperature range of FG Vir. The vertical line in each panel denotes a model whose radial fundamental frequency (F-mode) fits the observational frequency  $f_6 = 12.154$  c/d. Only models with masses  $1.815$ – $1.875 M_{\odot}$  fit the allowed temperature range

reference model with the input parameters:  $X = 0.70$ ,  $Z = 0.02$ ,  $d_{\text{over}} = 0$ ,  $\alpha = 1.0$ ,  $V_{\text{rot,ZAMS}} = 50$  km/s and OPAL opacities. To examine the effects of varying input parameters on the predicted frequency spectrum, all these and the stellar mass were varied, under the condition that  $F \equiv f_6$ .

The changes introduced by using different opacities or non-standard chemical composition were mainly compensated by changes in mass, in order to fulfill the only identification we use.

The main characteristics of twelve models of that series are given in Table 3. Model 2 differs from model 1 (our reference model) in mass; models 3, 4, 5 - in rotational velocity; model 6 versus 1 will demonstrate effect of changing the mixing-length parameter  $\alpha$ ; model 7 versus 1 will show effect of the overshooting; models 8 and 9 have non-standard chemical composition; finally, models 10, 11 and 12 differ from model 1 in opacity (additionally, overshooting is taken into account in the model 12).

Note the significantly larger spread in stellar mass between different models ( $1.72$ – $2.00 M_{\odot}$ ) than for the mass interval of  $1.815$ – $1.875 M_{\odot}$  in the case of the standard choice of input

parameters as was discussed in the previous subsection. The same is true for the mean density range: in Table 3 it varies between  $\bar{\rho}/\bar{\rho}_{\odot} = 0.1542$  and  $0.1597$  (or between  $0.1558$  and  $0.1584$  when using only OPAL opacities). This spread is at least one order of magnitude larger than for the standard input data. Nevertheless, this seismic estimate of the mean density, which is based both on the well determined effective temperature and the one identification we are using, provides a strong constraint on possible FG Vir models<sup>2</sup>.

We note that besides quite different stellar masses of  $1.7$ – $2.0 M_{\odot}$  (see Table 3) the evolutionary tracks for all 12 models in their MS-part lie well inside the region of  $1.80$ – $1.90 M_{\odot}$  of the standard set. Including a luminosity estimation  $\log(L/L_{\odot}) \approx 1.1$ – $1.2$  from trigonometric parallax determined by Hipparcos, all MS model tracks pass the error box, as well as the error box in the  $\log g$ - $\log T_{\text{eff}}$ -diagram. On the contrary, none of the post-MS models fits such a combination of parameters.

<sup>2</sup> For the multiperiodic  $\delta$  Scuti-type star XX Pyxidis, for example, there is no observational information about mode identification. Therefore it was necessary to consider a large number of models with very different mean densities (Pamyatnykh et al. 1998).

**Table 3.** Parameters of FG Vir models with  $\mathbf{F} \equiv f_6$ . The symbols have their usual meaning (see text). For the opacity,  $\kappa$ , the OPAL, OP or artificially modified OPAL data were used.  $p_1/p_4$  is the ratio of frequency of radial fundamental mode,  $f(p_1)$ , to that of third overtone,  $f(p_4)$

Model	$M/M_\odot$	$X$	$Z$	$\log T_{\text{eff}}$	$\log L$	$R/R_\odot$	$\log g$	$V_{\text{rot}}$	$\alpha$	$d_{\text{over}}$	$\kappa$	$\bar{\rho}/\bar{\rho}_\odot$	$p_1/p_4$
1	1.85	0.70	0.02	3.8760	1.1690	2.274	3.988	45	1.0	0.0	OPAL	0.1571	0.5236
2	1.82	0.70	0.02	3.8701	1.1406	2.261	3.985	45	1.0	0.0	OPAL	0.1571	0.5233
3	1.85	0.70	0.02	3.8761	1.1696	2.274	3.989	31	1.0	0.0	OPAL	0.1560	0.5231
4	1.85	0.70	0.02	3.8756	1.1676	2.274	3.983	67	1.0	0.0	OPAL	0.1570	0.5248
5	1.85	0.70	0.02	3.8753	1.1656	2.272	3.976	90	1.0	0.0	OPAL	0.1563	0.5266
6	1.85	0.70	0.02	3.8760	1.1691	2.274	3.988	45	2.0	0.0	OPAL	0.1570	0.5236
7	1.85	0.70	0.02	3.8796	1.1837	2.275	3.987	45	1.0	0.2	OPAL	0.1558	0.5231
8	1.85	0.65	0.03	3.8734	1.1562	2.267	3.990	45	1.0	0.0	OPAL	0.1584	0.5227
9	2.00	0.70	0.03	3.8748	1.1844	2.327	4.001	46	1.0	0.0	OPAL	0.1574	0.5231
10	1.72	0.70	0.02	3.8754	1.1507	2.233	3.972	45	1.0	0.0	OP	0.1542	0.5262
11	1.95	0.70	0.02	3.8712	1.1600	2.301	4.000	45	1.0	0.0	mod.OPAL	0.1588	0.5204
12	1.95	0.70	0.02	3.8746	1.1738	2.301	4.002	32	1.0	0.2	mod.OPAL	0.1597	0.5195

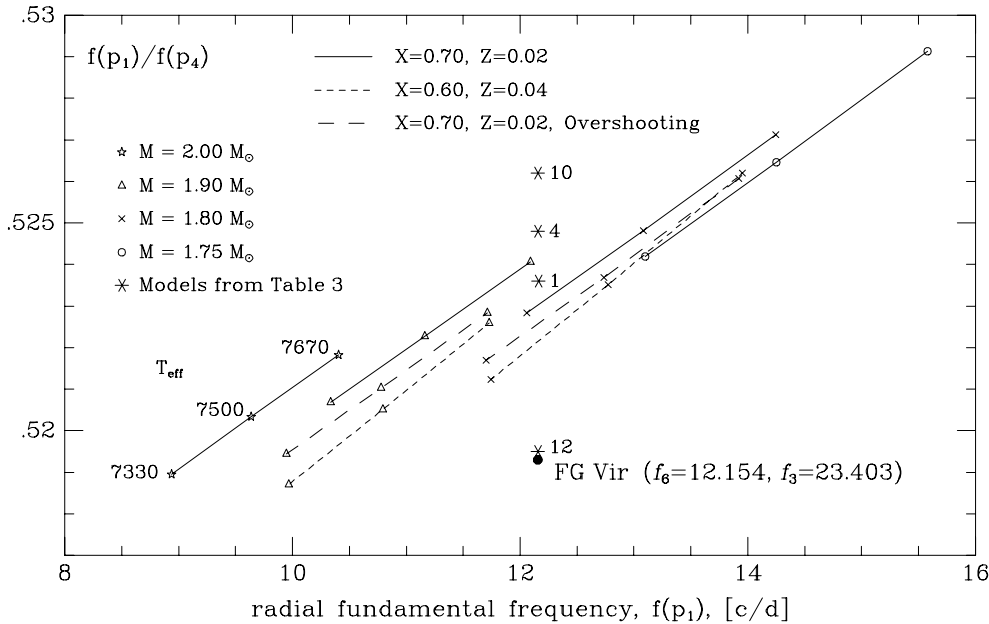


**Fig. 6.** Frequency ratio of the radial fundamental mode to the third overtone for a wide range of parameters of  $\delta$  Scuti star models and of some FG Vir models from Table 3 (asterisks). The large filled circle corresponds to the observed frequency ratio,  $f_6/f_3$ , of 0.5193. Only the models with artificially modified opacities (such as model 12 of Table 3) can fit the observed ratio

#### 4.4. The problem of the radial frequency ratio

Viskum et al. (1998) identified  $f_3$  as a radial mode. We note here that the phase-difference method presented earlier in this paper allows both  $\ell = 0$  and 1 for  $f_3$ , i. e. radial as well as nonradial pulsation. We will now examine the radial hypothesis. In the last column of Table 3 the ratio of frequencies of the radial fundamental mode,  $p_1$ , and of the third overtone,  $p_4$ , is given ( $f(p_1)/f(p_4)$ ). For models 1–10 these values are close to, but not equal to the observed ratio of  $f_6/f_3 = 0.5193$ , independent of which parameter was changed. This can also be seen in Fig. 6, where the ratio  $f(p_1)/f(p_4)$ , is plotted against  $f(p_1)$  for a wide range of parameters of  $\delta$  Scuti star models. There are well-defined monotonic variations of this ratio with changing mass, effective temperature or chemical composition, but the observed ratio disagrees with all these results.

The only exception is the model 12 with artificial opacities, which was constructed in the following way. For FG Vir

models, the frequency ratio is most sensitive to the choice of opacities as it can be seen from comparison of models 10 and 1 (OP versus OPAL opacities). Physically, OP data differ from those of OPAL by underestimation of collective effects in stellar plasma, therefore OP opacities are systematically lower than OPAL in deep stellar interiors. For FG Vir models, this difference in opacity is about 20% at temperatures above  $10^6$  K. In the envelope, at lower temperatures, OP opacity varies slightly more monotonously along radius than does OPAL opacity: some dips are slightly shallower and some bumps are more flat. The differences do not exceed 8%: for example, at a temperature of 14 000 K the OP opacity is 4% smaller and at a temperature of 300 000 K it is 7.5% higher than the OPAL opacity.

Using the fact that the difference in frequency ratios between model 1 (OPAL) and model 10 (OP) is comparable with the difference between model 1 and the observations (but these differences are of opposite sign, see Fig. 7), we performed a very simple numerical experiment: we artificially scaled OPAL opac-

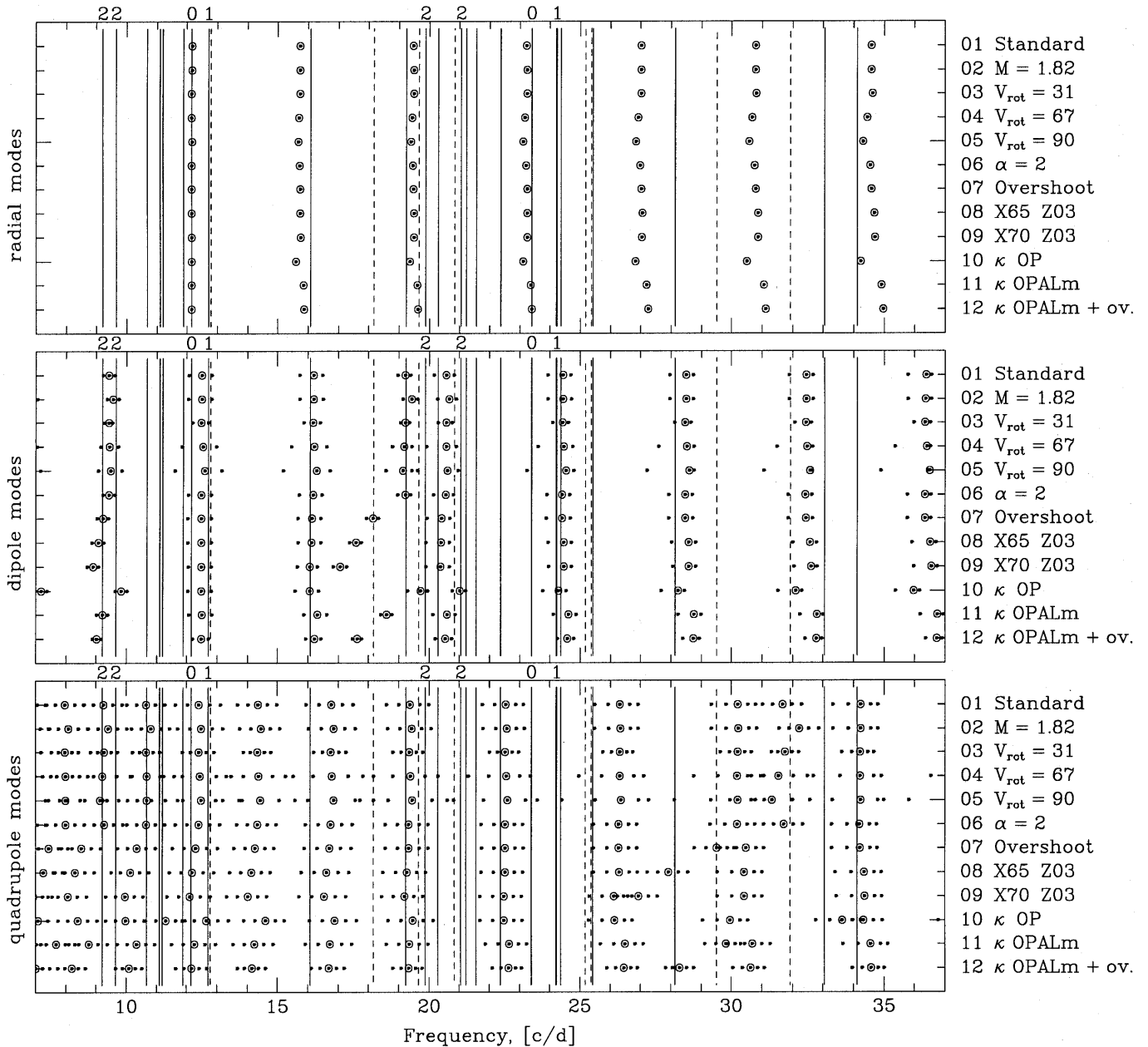


**Fig. 7.** Frequency spectra of radial, dipole and quadrupole oscillations of various FG Vir models. Axisymmetric modes ( $m = 0$ ) are marked by enlarged circles. Model numbers (see Table 3 for parameters) together with some model indicators are given to the right of the panels. Vertical solid and dashed lines correspond to observed frequencies – statistically significant and probable, respectively. Numbers above some observed frequencies give identifications for the degree of the modes ( $\ell$ ) based on multicolor photometry data and on the results by Viskum et al. (1998)

ities with a factor, which is the ratio of OPAL to OP data. More clearly, we used  $\kappa_{\text{modified}} = \kappa_{\text{OPAL}} \cdot [\kappa_{\text{OPAL}}/\kappa_{\text{OP}}]$ . Models 11 and 12 were constructed using  $\kappa_{\text{modified}}$ . For model 12 we additionally set  $d_{\text{over}}$  to  $0.2 H_p$  and lowered the rotational velocity. This model fits the observed frequency ratio very nicely as demonstrated in Fig. 7. However, this agreement should not be construed as an indicator for a new revision of atomic physics data on opacity, since the mode identification from Viskum et al. (1998) may not be unique due to the size of the error bars. Moreover, we cannot exclude additional effects like nonlinear mode interaction or rotational mode coupling, which may influence

the frequency spectrum. In the last section the problem of rotational mode coupling will be briefly discussed. The observed variability of the amplitude of mode  $f_3$  is another argument in favour of possible nonlinear mode interaction.

Viskum et al. (1998) were able to interpret the observed frequency ratio  $f_6/f_3 = 0.5193$  as the radial frequency ratio  $f(p_1)/f(p_4)$ . They did not construct full evolutionary models but scaled a model of  $2.2M_{\odot}$ , which was selected to match the observed frequency ratio with the radial frequency ratio  $f(p_1)/f(p_4)$ . Using the homology argument, they estimated the mean density of the true FG Vir model by multiplying

the mean density of the  $2.2M_{\odot}$  model by the square of the ratio  $f_{\text{obs}}/f_{\text{model}}$ . In such a way an agreement between observed frequencies  $f_6$ ,  $f_3$  and a pair of radial modes of the scaled model was achieved by definition. The estimated gravity, luminosity and distance of the scaled model were found to be in good agreement with the photometric and the spectroscopic data and with the Hipparcos parallax. The authors noted that the high precision of their asteroseismic density estimate ( $\bar{\rho}/\bar{\rho}_{\odot} = 0.1645 \pm 0.0005$ ) is based on a fixed (solar) metallicity for FG Vir. Indeed, with our standard choice of chemical abundances and opacity and assuming the fit  $\mathbf{F} \equiv f_6$  we estimated the mean density of the FG Vir model with even five times higher accuracy (see Sect. 4.2), but possible variations of the global parameters result in at least one order of magnitude worse precision of this estimate.

#### 4.5. Theoretical frequency spectra versus observations

Frequency spectra of radial, dipole and quadrupole modes for all 12 models from Table 3 are shown in Fig. 7. The effects of different choices of input parameters can be estimated by comparison of the results for different models. We discuss here both general properties and some peculiarities of these frequency spectra.

For nonradial oscillations, evolutionary overlapping of frequency intervals of g- and p-modes (see Fig. 5) results in avoided crossings, which disturb the approximately equidistant frequency spacing between acoustic multiplets. Gravity and mixed modes are very sensitive to the interior structure as can be seen for models of different chemical composition, different opacities and for models with and without overshooting. On the contrary, the change of  $\alpha$  (model 6 versus model 1) has a negligible influence on the frequency spectrum due to ineffective convection in the relatively hot envelope of FG Vir.

Rotation splits nonradial multiplets and strongly complicates the frequency spectra. Except for models with slowest rotation, we observe a forest of quadrupole modes in the low-frequency part of the interval, with overlapping components of the different multiplets. The common property of the spectra is a large asymmetry of the rotational splitting, which is caused by the second-order effects of rotation (Dziembowski & Goode 1992). The asymmetry is higher the higher the order of the p-modes is.

It is not trivial to select a model reproducing the observed frequencies exactly. Simple attempts to minimize frequency differences (O-C) by a combined variation of input parameters of the reference model fail due to strong and non-linear sensitivity of gravity modes to interior structure. At the same time, this strong sensitivity may help to fit some chosen frequencies without changing the rest of the spectrum, (cf. models 1 and 7, for example). It is obvious from Fig. 7 that generally it is much easier to fit a low-frequency mode than a high-frequency mode, because the spectrum is more dense at lower frequencies. For some of the observed modes there is no satisfactory  $\ell = 0 - 2$  solution: see, for example, the group  $f_4, f_{14}, f_{18}$  around 21 c/d or  $f_{17}$  at 33 c/d. Besides geometric cancellation, there are no

objections to identify frequencies in the gaps with modes of degree  $\ell=3$  and  $\ell=4$ . Note that even for  $\ell = 0 - 2$  the number of unstable modes is a few times larger than the observed one: in the observational frequency interval there are 6–7 radial modes, 24 dipole modes and 50–55 quadrupole modes. Therefore, a presently unknown mode selection mechanism must exist.

Note that most of the models presented in Fig. 7 show a good fit of the dominant observed mode  $f_1$  (12.716 c/d) with  $\ell = 1$  mode of  $m = -1$  or 0. This is in agreement with the mode identification from photometric phase differences. On the contrary, it is quite difficult to achieve a similar fit with a dipole mode for the observed mode  $f_3$  (23.403 c/d). In Table 4 we present some results to quantify the fitting of 21 modes (corresponding to the observed frequencies  $f_1$  through  $f_{22}$ , omitting  $f_{16}$ ) for models 1 (reference model), 3 (low rotation), 8 ( $X = 0.65$ ,  $Z = 0.03$ ) and 12 (artificially modified opacity + overshooting). In the cases of close observed frequencies (for example,  $f_1, f_{11}, f_{21}$  around 24 c/d, or  $f_4, f_{14}, f_{18}$  around 21 c/d) we give a few possible identifications for each frequency. Moreover, if there is no  $\ell = 0 - 2$  mode for a given observed frequency, we show the closest mode of  $\ell = 3$  or 4: the frequency spectrum of these modes is so dense that practically everywhere in the observed interval a fitting within 0.1 c/d is possible.

Model 12 seems to be the best-fitting model in our series. Note the excellent agreements in both frequency and  $\ell$ -identifications for all ten dominant frequencies. The mean difference (O-C) is about 0.04 c/d for these modes. The fit for most of the remaining frequencies is also good, once  $\ell = 3$   $\ell = 4$  modes are considered. Possible discrepancies at low frequencies do not appear serious to us due to the strong sensitivity of g-modes to model parameters. Because of the effects of avoided crossing some of the quadrupole modes of higher order are also quite sensitive to small variations of parameters (cf.  $\ell = 2$  modes for models 1 and 2 at approximately 32 c/d).

In Fig. 8 we compare the range of observed frequencies and of excited modes explicitly for the reference model as well as three other models. FG Vir is located in the HR-diagram in the middle of the instability strip (see, for example, Breger & Pamyatnykh 1998). Consequently, the driving of oscillations is effective in a wide frequency region which extends over 7 radial overtones. The independence of the driving efficiency on the mode degree,  $\ell$ , is typical for the oscillations excited by the opacity mechanism.

We also note that the observed frequency spectrum is divided clearly into two groups: at 9-13 c/d and at 19-25 c/d. However, the present models do not predict any instability gap in frequency, as can be seen in Fig. 8.

#### 4.6. Rotational mode coupling

An additional factor which influences the frequencies of a rotating star is the coupling between modes with close frequencies whose azimuthal orders,  $m$ , are the same and whose degrees,  $\ell$ , are also the same or differ by 2. The effect was described and discussed in detail by Dziembowski & Goode (1992) and by Soufi et al. (1998). The frequency distance between two

**Table 4.** Best fits for some FG Vir models

Observations			Model 1				Model 3				Model 8				Model 12			
N	$f$ [c/d]	id.	$\ell$	$m$	$f$ [c/d]	O-C	$\ell$	$m$	$f$ [c/d]	O-C	$\ell$	$m$	$f$ [c/d]	O-C	$\ell$	$m$	$f$ [c/d]	O-C
1	12.716	1	1	-1	12.821	.105	1	-1	12.714	.002	1	-1	12.814	.098	1	-1	12.719	.003
			2	-1	12.770	.054												
2	24.228	2/1	1	0	24.436	.208	1	1	24.083	.145	1	0	24.453	.225	1	1	24.250	.022
			3	-2	24.331	.103	3	-2	24.128	.100	3	-2	24.381	.153	3	-2	24.308	.080
3	23.403	0	0	0	23.226	.177	0	0	23.237	.166	0	0	23.247	.156	0	0	23.402	.001
			3	1	23.285	.118	3	1	23.317	.086								
4	21.052	2	1	-1	20.828	.224	1	-1	20.758	.294	1	-1	20.667	.385	1	-1	20.739	.313
			2	2	21.767	.715	2	2	22.005	.953	2	2	21.723	.671	2	2	22.106	.054
			3	-2	21.079	.027	3	-3	21.092	.040	3	-2	20.961	.091	3	-3	21.024	.028
			4	-3	21.048	.004	4	1	21.091	.039	4	-3	21.037	.015	4	-4	21.085	.033
5	19.868	2	2	-2	19.996	.128	2	-2	19.800	.068	1	1	19.893	.025	2	-2	19.774	.094
			2	-2	19.996	.128	2	-2	19.800	.068	2	-2	19.899	.031				
6	12.154	0	0	0	12.161	.007	0	0	12.156	.002	0	0	12.152	.002	0	0	12.157	.003
7	9.656	1/2	1	-1	9.609	.047	2	-2	9.705	.049	1	-1	9.250	.406	2	2	9.656	.000
			2	-1	9.556	.100					2	1	9.815	.159				
											3	-3	9.661	.005				
8	9.199	2	1	1	9.228	.029	2	0	9.267	.068	1	-1	9.250	.051	1	-1	9.143	.056
			2	0	9.242	.043	2	-2	8.940	.259								
9	19.228	(0)	1	0	19.204	.024	1	0	19.217	.011	2	0	19.265	.037	2	0	19.326	.098
10	20.288	(1)	1	1	20.162	.126	1	1	20.293	.005	1	0	20.385	.097	1	1	20.206	.082
			3	0	20.333	.045												
11	24.200	-	1	0	24.436	.236	1	1	24.083	.117	1	0	24.453	.253	1	1	24.250	.050
			3	-2	24.331	.131	3	-2	24.128	.072	4	1	24.074	.126	3	-2	24.308	.108
12	16.074	-	1	0	16.191	.117	1	0	16.170	.096	1	0	16.124	.050	1	0	16.211	.137
			2	2	15.946	.128	3	-1	16.079	.005	3	-1	16.016	.058	2	2	16.123	.049
			4	0	16.060	.014	4	0	16.082	.008	4	-1	16.010	.064	4	2	16.114	.040
13	34.119	-	2	0	34.231	.112	2	0	34.221	.102	2	1	33.916	.203	2	2	33.970	.149
			3	-2	34.231	.112	3	-2	34.172	.053	3	0	34.019	.100				
14	21.232	-	1	-1	20.828	.404	1	-1	20.758	.474	1	-1	20.667	.565	1	-1	20.739	.493
			3	-2	21.079	.153	3	-3	21.092	.140	2	2	21.723	.491	3	-3	21.024	.208
			4	-4	21.368	.136	4	0	21.367	.135	4	0	21.167	.065	4	0	21.147	.085
15	11.110	-	2	-1	10.975	.135	2	-2	11.099	.011	2	2	11.423	.313	2	2	11.649	.539
			3	2	11.099	.011	3	-2	11.074	.036	3	0	10.942	.168	3	-1	11.024	.086
			4	0	11.092	.018	4	0	11.085	.025	4	4	10.983	.127	4	2	11.059	.051
17	33.056	-	2	2	33.316	.260	1	-1	32.609	.447	1	-1	32.785	.271	1	-1	32.959	.097
			4	-1	33.020	.036	4	-2	33.152	.096	3	1	33.092	.036	4	0	33.032	.024
18	21.551	-	2	2	21.767	.216	2	2	22.005	.454	2	2	21.723	.172	2	2	22.106	.555
			3	-3	21.433	.118	4	-1	21.642	.091	4	-1	21.566	.015	4	-1	21.421	.130
19	28.140	-	1	1	27.959	.181	1	1	28.125	.015	2	-1	28.247	.107	2	1	28.062	.078
			4	1	28.205	.065	3	-2	28.133	.007	3	-1	28.101	.039	3	-1	28.163	.023
20	11.195	-	2	-2	11.277	.082	2	-2	11.099	.096	2	2	11.423	.228	2	2	11.649	.454
			3	-2	11.281	.086	3	-3	11.309	.114	3	-1	11.289	.094	3	3	11.223	.028
			4	2	11.231	.036	4	3	11.181	.014	4	-2	11.285	.090	4	4	11.175	.020
21	24.354	-	1	0	24.436	.082	1	0	24.413	.059	1	0	24.453	.099	1	1	24.250	.104
			3	-2	24.331	.023	3	-3	24.349	.005	3	-2	24.381	.027	3	-2	24.308	.046
			4	0	24.398	.044					4	0	24.457	.103	4	1	24.339	.015
22	11.870	-	2	1	12.029	.159	2	2	11.859	.011	2	1	11.818	.052	2	1	11.915	.045
			4	4	11.846	.024					3	-3	11.969	.099				

near-degenerate modes increases when coupling is taken into account. The significance of this rotational frequency perturbation was demonstrated by Pamyatnykh et al. (1998) in application to XX Pyx. It was shown that at rotational velocity of about 90 km/s the frequency shifts of coupled radial and quadrupole

(or dipole and octupole) overtones achieve 0.1–0.2 c/d. Therefore, in particular, a significant change of radial frequency ratios may be expected.

We estimated this effect in some of our FG Vir models and found it to be unimportant at rotational velocities of about and

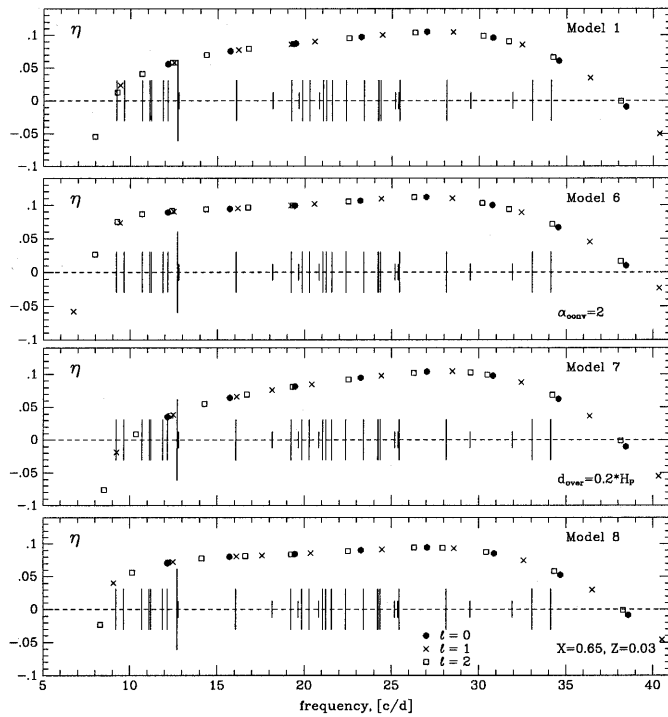


**Fig. 8.** Normalized growth-rates,  $\eta$ , of low-degree oscillation modes of some FG Vir models from Table 4. Only axisymmetric modes ( $m = 0$ ) are shown. Positive values correspond to unstable modes. Vertical lines mark observed frequencies from Table 1, probable frequencies  $f_{25}$  to  $f_{32}$  are shorter. The longest line at 12.716 c/d corresponds to the mode  $f_1$  with the highest amplitude

less than 45 km/s. For example, for the reference model 1, the frequencies of the radial fundamental mode,  $f(p_1)$ , and of the third overtone,  $f(p_4)$ , are changed due to coupling with closest axisymmetric quadrupole modes by  $-0.0035$  c/d and  $0.0091$  c/d, respectively. The effect is much stronger for more rapidly rotating models: for model 5 with  $V_{\text{rot}} = 90$  km/s, the radial fundamental mode and third overtone are shifted by  $-0.0436$  c/d and  $0.1545$  c/d, respectively, which results in the change of the frequency ratio from 0.5266 to 0.5212. As another example, we were able to reproduce the observed ratio  $f_6/f_3 = 0.5193$  as the radial frequency ratio for a model with initial abundances  $X = 0.65$ ,  $Z = 0.03$  and with  $V_{\text{rot}} = 91$ – $92$  km/s. However, the rapid rotation seems to be rather improbable for FG Vir with  $v \sin i = 21 \pm 1$  km/s, as it was discussed by Viskum et al. (1998).

Note that the coupling effect is higher for higher overtones: for model 5, the shift of the radial sixth overtone frequency (34.306 c/d) is 0.520 c/d due to interaction with the closest axisymmetric quadrupole mode of 34.219 c/d which is shifted by the same quantity 0.520 c/d in the opposite direction. Moreover,  $\ell = 2$  modes are affected by coupling with  $\ell = 4$  modes, and so on. We conclude that for rapidly rotating models it is necessary to take the rotational coupling into account in attempts to fit the observed frequency spectrum with the theoretical one.

The rotational coupling results also in a mutual contamination of amplitudes of spherical harmonic components of in-

teracting modes (Soufi et al 1998, see examples in Table 4 of Pamyatnykh et al. 1998). This adversely affects the mode discrimination by means of multicolor photometry (see the footnote in Sect. 3) and should influence spectroscopic determinations as well. However, this effect was found to be important only in models with more rapid rotation than found for FG Vir. A more detailed discussion of the rotational mode coupling problem in connection with the interpretation of the observed multifrequency spectrum will be given by Dziembowski & Goupil (1998).

*Acknowledgements.* We are grateful to M. Viskum and S. Frandsen for making the photometry used in their FG Vir paper available to us and W. Dziembowski for stimulating discussions. Part of the investigation has been supported by the Austrian Fonds zur Förderung der wissenschaftlichen Forschung, project number S7304. AAP acknowledges partial financial support by the Polish Committee for Scientific Research (grant 2-P03D-014-14) and by the Russian Foundation for Basic Research (grant 98-02-16734).

## References

- Aizenman M.L., Smeyers P., Weigert A., 1977, A&A 58, 41  
 Alexander D.R., Ferguson J.W., 1994, ApJ 437, 879  
 Bedding T.R., Kjeldsen H., Reetz J., Barbuy B., 1996, MNRAS 280, 1155  
 Breger M., 1990a, Comm. Asteroseismology (Vienna) 20, 1  
 Breger M., 1990b, A&A 240, 308  
 Breger M., Handler G., 1993, Baltic Astronomy 2, 468  
 Breger M., Stich J., Garrido R., et al., 1993, A&A 271, 482  
 Breger M., Handler G., Nather R.E., et al., 1995, A&A 297, 473 (Paper I)  
 Breger M., Pamyatnykh A.A., 1998, A&A 332, 958  
 Breger M., Zima W., Handler G., et al., 1998, A&A 331, 271  
 Dziembowski W.A., 1977, Acta Astron. 27, 95  
 Dziembowski W.A., Goode P.R., 1992, ApJ 394, 670  
 Dziembowski W.A., Goupil M.-J., 1998, in preparation  
 Dziembowski W.A., Pamyatnykh A.A., 1991, A&A 248, L11  
 Garrido R., Garcia-Lobo E., Rodriguez E., 1990, A&A 234, 262  
 Grevesse N., Noels A., 1993, In: Pratzto N., Vangioni-Flam E., Casse M. (eds.) Origin and Evolution of the Elements. Cambridge Univ. Press., p. 15  
 Guzik J.A., Templeton M.R., Bradley P.A., 1998, ASPC 135, 470  
 Handler G., Pikall H., O'Donoghue D., et al., 1997, MNRAS 286, 303  
 Iglesias C.A., Rogers F.J., 1996, ApJ 464, 943  
 Kurucz R.L., 1993, CD-ROM 1-23, Smithsonian Astrophysical Observatory  
 Mantegazza L., Poretti E., Bossi M., 1994, A&A 287, 95  
 Osaki Y., 1975, Publ. Astron. Soc. Japan 27, 237  
 Pamyatnykh A.A., Dziembowski W.A., Handler G., Pikall H., 1998, A&A 333, 141  
 Rogers F.J., Swenson F.J., Iglesias C.A., 1996, ApJ 456, 902  
 Seaton M.J., 1996, MNRAS 279, 95  
 Soufi F., Goupil M.-J., Dziembowski W.A., 1998, A&A 334, 911  
 Stankov A., Ashley M.C.B., Mreger M., Prouton O., 1998, ApSS, in press  
 Unno W., Osaki Y., Ando H., et al., 1989, Nonradial oscillations of stars. University of Tokyo Press  
 Vandakurov Yu.V., 1967, Astron. Zh. 44, 786  
 Viskum M., 1997, PhD thesis, Aarhus Universiteit  
 Viskum M., Kjeldsen H., Bedding T.R., et al., 1998, A&A 335, 549  
 Watson R.D., 1988, ApSS 140, 255  
 Winget D.E., Nather R.E., Clemens J.C., 1991, ApJ 378, 326